Hydrogen Evolution Reaction for Vacancy-Ordered i-MXenes and the Impact of Proton Absorption into the Vacancies

(article starts on next page)

Hydrogen Evolution Reaction for Vacancy-Ordered i-MXenes and the Impact of Proton Absorption into the Vacancies

*Hans Lind, Björn Wickman, Joseph Halim, Gerard Montserrat-Sisó, Anders Hellman, and Johanna Rosen**

A study of the hydrogen evolution reaction (HER) for Mo-, W-, and Nb-based MXenes is presented, where $W_{1.33}C$ MXene with ordered vacancies is chosen for further investigation. The electrochemical measurements show that if the $W_{1.33}C$ MXene is subjected to high cathodic potentials, it greatly improves the activity and onset potential for the HER. The enhancement continues to improve independent of whether the potential is kept fixed at a certain cathodic potential or if the potential is scanned repeatedly. Interestingly, the improvement disappears if the material is subjected to anodic potential. Based on these observations, the hydrogen interaction with the MXene surface as well as in the vacancies is investigated by means of first-principles calculations. These show that the adsorption energy of hydrogen is sensitive to both surface coverage and vacancy occupancy, and that, for certain structures with hydrogen in the vacancies, thermoneutral values of hydrogen adsorption can be obtained. Based on the calculations it is argued that under high cathodic potentials, protons can transfer to the vacancies and stay there in a metastable state as hydrogen atoms, while at anodic potential the process is reversed. The first-principles results provide a rationale for the strongly enhanced HER activity observed experimentally on $W_{1.33}C$ MXene.

1. Introduction

2D materials have attracted tremendous interest over the last decade owing to their extraordinary electronic, chemical, optical, mechanical, and structural properties that result from their reduced dimensionality compared to their bulk 3D counterparts. 2D transition metal carbides and nitrides, also known as MXenes,[1,2] are a comparatively young class of 2D materials formed by etching the parent 3D MAX phases,[3] $M_{n+1}AX_n$ (n = 1–3), where M is an early transition metal, A is an A-group element, and X is carbon or nitrogen. MAX phases are atomically laminated compounds of a hexagonal structure, and selective etching of the A layer, typically Al, leaves 2D MXene sheets of a general formula $M_{n+1}X_nT_z$, where T_z are surface terminations formed upon etching (commonly O, OH, and/or F), and z is the number of terminations per formula unit. There are more than 20 MXenes identified to date, and they have demonstrated a large potential for numerous applications, including hydrogen and energy storage,[4,5] transparent conducting electrodes,[6] and electromagnetic interference shielding.[7]

Compared to many other 2D materials MXenes stands out, since they are both hydrophilic and conducting. Moreover, they are tailorable through the large number of attainable MXene compositions, or through surface functionalization (control of terminations). Recently, a third route for property tuning was presented in the form of MXenes with ordered vacancies.[8–10] These materials are obtained from parent quaternary i-MAX phases, $(M'_{2/3}M''_{1/3})_2AX$, which through "targeted etching," i.e., removal of the A-layer combined with the alloying M" element, form a MXene with ordered vacancies.[10] These MXenes have shown promise for primarily supercapacitor applications,[8,10] but also for water desalination[11] and hydrogen production via the hydrogen evolution reaction (HER).[9]

Traditional MXenes without ordered vacancies have been subject to theoretical[12–14] and experimental[15] investigations related to HER. For instance, it has been demonstrated that Mo_2C has a close to optimal hydrogen adsorption energy, and consequently an overpotential near zero, making it a promising candidate for HER catalyst.[16] Another study showed that the introduction of impurities such as Pt or Co in the surface layer of the MXene can further increase its potential as a catalyst for hydrogen production.[17,18] Surface functionalization of the MXenes has been shown to be of high importance for the hydrogen evolution, e.g., indicating that F terminations on

Dr. H. Lind, Dr. J. Halim, Prof. J. Rosen
Thin Films Physics
Department of Physics, Chemistry, and Biology
Linköping University
Linköping SE-581-83, Sweden
E-mail: johanna.rosen@liu.se
Prof. B. Wickman, G. Montserrat-Sisó
Department of Physics
Chalmers University of Technology
Gothenburg 412 96, Sweden
Prof. A. Hellman
Department of Physics and Competence Centre for Catalysis
Chalmers University of Technology
Gothenburg 412 96, Sweden

**ADVANCED
SCIENCE NEWS**

www.advancedsciencenews.com

**ADVANCED
SUSTAINABLE
SYSTEMS**

www.advsustainsys.com

Ti_3C_2 can be detrimental to the adsorption energy of hydrogen, compared to O.[19] Meanwhile, other works have presented F free growth of Ti_3C_2 MXene with improved electric and catalytic properties, compared to ones etched with HF acid.[20,21] In addition, it has been reported that analysis of V_4C_3 in a repeated hydrogen evolution process improved the value of the overpotential, supposedly thanks to changes in functionalization.[22]

The above studies are spurred by the need for affordable, reliable, sustainable and environmentally friendly methods for energy production and storage, including catalytic reactions such as HER. A good HER catalyst is a stable material, with an optimal binding energy of adsorbed hydrogen atoms.[23] Currently the best catalyst for the HER is platinum, but new and cheaper catalysts comprised of abundant materials are highly sought after. Alternatives considered include 2D materials,[24–26] which display a high surface to volume ratio, and where MXenes are one of the most recent additions. Theoretical simulations suggest that MXene materials in general,[14,27] and the hypothetical W_2C in particular,[12] can fulfill both of these crucial requirements. Pan used density functional theory (DFT) to calculate the H adsorption free energy, ΔG_{ad}, and predicted that the hypothetical W_2C should even have a HER activity rivaling that of Pt as the coverage dependent ΔG_{ad} approaches thermoneutral.[12] Most recently, we realized the first W-based MXene, $W_{1.33}C$, derived from a new i-MAX phase,[9] and initial HER analysis showed a clear catalytic activity toward HER.[9]

Given these early indications, along with the need to identify new and cheap/abundant materials for HER, we have chosen to conduct a more detailed experimental and theoretical investigation into such properties. As a starting point, we experimentally investigate HER from W-, Mo-, and Nb-based MXenes. The vacancy-ordered $W_{1.33}C$ MXene stands out and is therefore investigated in more detail through a combined theoretical and experimental approach. In particular, we explore how the vacancies of $W_{1.33}C$ influence the ability of the MXene to both store hydrogen and catalyze HER by considering H functionalization on top of the O atoms, as well as inside the vacancies. We look at the experimentally observed hydrogen evolution activities alongside calculated values on the adsorption energies and thermodynamic stability for different ratios of hydrogen adsorption. We find both a very high hydrogen evolution current in $W_{1.33}C$, as well as a lowering of the onset potential by subjecting the material to repeated potential cycling to high cathodic potential. The first-principles calculations show that hydrogen bound inside the vacancies will result in improved onset potential, and thanks to the metastable nature of these vacancy sites provides an explanation to the reversible enhancement of the onset potential.

2. Results and Discussion

2.1. Experimental Hydrogen Evolution Reaction on MXenes

The activity of the MXene materials toward HER was evaluated in 0.5 M H_2SO_4 and the results are shown in **Figure 1**, where we have also added results from a polycrystalline Pt and a bare glassy carbon electrode, for comparison. As can be seen, the glassy carbon substrate has virtually no activity for the HER in the potential window of Figure 1, while Pt is very

close to an ideal catalyst for this reaction. Among the MXene materials, clear differences in HER activity can be seen. The $Nb_{1.33}C$ shows the lowest HER activity, followed by the Mo_2C and the two $Mo_{1.33}C$, while the two $W_{1.33}C$ samples show the highest HER activity among the evaluated MXenes. The real surface area of the MXene materials was estimated from electrochemical capacitance measurements and revealed an area about eight times larger than the projected surface area (i.e., the surface area of the glassy carbon disk) for all MXenes (see the Supporting Information for further discussion). It should also be mentioned that for some samples, the HER activity was changing while performing the electrochemical measurements. For the $Nb_{1.33}C$ and Mo_2C samples, the HER activity was rather constant and changed only slightly with repeated cycling. For the $Mo_{1.33}C$ and the $W_{1.33}C$ samples, an increased HER activity was observed with repeated cycling and polarization at cathodic potentials. This kind of improvement in HER is rather rare, but documented for similar materials.[8,14,16] The fact that the HER activity can be significantly improved from the as-prepared material raises questions on the mechanisms involved and the potential for improvement. Although the materials are not rivalling Pt in efficiency to date, a deeper understanding of the materials and mechanisms will hopefully result in cheap catalysts made from earth abundant materials with a high enough activity. The effect appeared most pronounced on the $W_{1.33}C$ samples, motivating the here performed more systematic analysis of the changes in the HER activity and onset potential.

2.2. Onset Potential of the HER on $W_{1.33}C$

In the experimental HER analysis, the onset potential was defined as the potential where the current crossed −1 mA cm^{-2} based on the projected (also termed geometric) surface area. The value of the onset potential was found to change
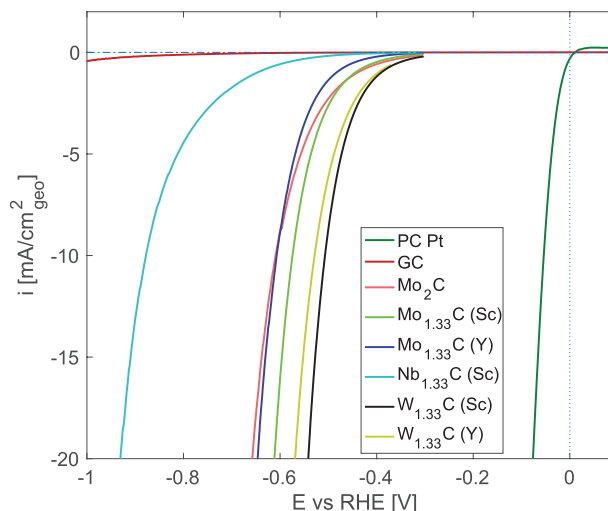

Figure 1. Hydrogen evolution reaction for different MXenes, with Pt and glassy carbon (GC) for comparison. Pt, to the far right is a near perfect catalyst for HER, while GC has virtually no activity. The parenthesis in the legend entries indicates whether the MXene was exfoliated from a Sc or Y based MAX phase.
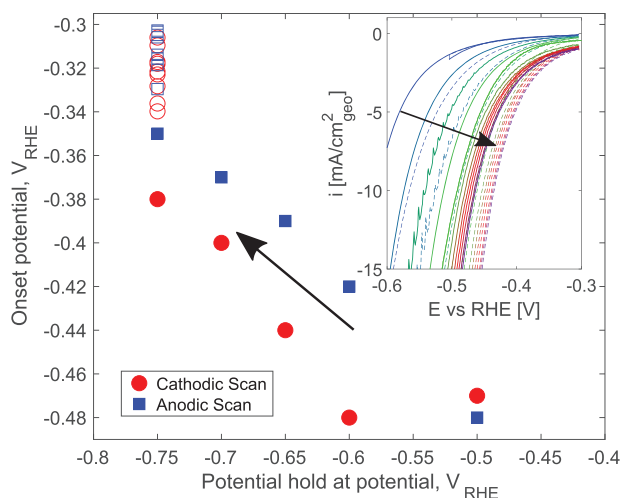
Figure 2. Onset potential for the HER on $W_{1.33}C$ before and after potential holds of 5 min at different cathodic potentials. Filled symbols represent measurements where the potential was changed between holds from -0.5 to -0.75 V_{RHE} where the cathodic scan data represents the onset before each hold and the anodic scan data represents the onset after each hold. Open symbols represent measurements of repeated holds at -0.75 V_{RHE}. In the inset, the solid lines mark the cathodic scan and the dashed lines mark the anodic with different colors for each sweep. Note that the first curve only goes down to -0.5 V_{RHE} before turning anodic, that way it looks like a notch on what is actually the second curve. In both the main figure, and the inset, the arrow indicates the direction of shifts over repeated cycles.

drastically depending on the electrochemical conditions, i.e., to what potential and duration the $W_{1.33}C$ samples were subject to. **Figure 2** shows the results from a measurement where the potential was scanned at 50 mV s^{-1} from -0.3 V_{RHE} and cathodically to different potentials where it was held for 5 min, starting at -0.5 V_{RHE} and finishing at -0.75 V_{RHE}. For each cycle (cathodic scan, hold, anodic scan) the onset potential was evaluated two times, first on the cathodic and then on the anodic scan. Thus, the cathodic onset represents the onset potential measured before the hold and the anodic onset represents the onset potential after the hold for each potential. The results from these measurements are shown with filled symbols in Figure 2. As can be seen, the onset potential starts at about -0.48 V_{RHE} and then shifts about 30–40 mV in anodic direction after each 5 min potential hold. It was also observed that the current did not completely stabilize during the 5 min holds and, thus, the values presented in Figure 2 do not represent absolute equilibrium. When reaching the cathodic hold potential of -0.75 V_{RHE}, we attempted to reach equilibrium by repeating the 5 min hold at -0.75 V_{RHE}, with scanning up to -0.3 V_{RHE} and back again until the current during the hold had stabilized. The onset potentials for these measurements are shown in open symbols in Figure 2. During the repeated holds, the anodic and cathodic onsets continue to shift toward more anodic values and the difference between them becomes smaller and smaller. After about 10 holds at -0.75 V_{RHE}, the current was more than twice as high as at the beginning of the first hold and was almost constant during the hold. In addition, there was virtually no difference between the anodic and cathodic onset potential, and a minimum value close
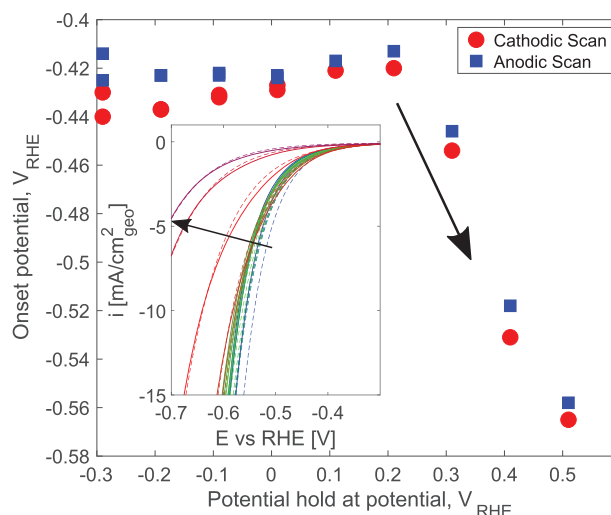

Figure 3. Onset potential for the HER on $W_{1.33}C$ upon changing the anodic potential during cyclic voltammetry. In the inset, the solid lines mark the cathodic scan and the dashed the anodic with different colors for each sweep. The arrows mark the shifts over repeated cycles.

to -0.3 V_{RHE} was determined for the onset potential. That means that the onset potential shifted in the anodic direction almost 0.2 V as a result of subjecting the $W_{1.33}C$ to cathodic potentials down to -0.75 V_{RHE}.

It should be noted that the $W_{1.33}C$ sample produced very large currents thanks to the HER during the potential holds. The maximum HER current at -0.75 V_{RHE} obtained when the onset potential in Figure 2 had stabilized was about 1 A cm^{-2}. This is a very high number, compared to, e.g., ref. [28], especially when considering that the capacitance measurements suggested that the roughness factor for the $W_{1.33}C$ sample was merely 8.2 (see the Supporting Information for further discussion).

Another interesting observation is that when the $W_{1.33}C$ sample was cycled at 50 mV s^{-1} between a cathodic potential of -0.7 V_{RHE} and an upper potential limit that was varied from -0.3 to 0.5 V_{RHE} we find a clear shift in the cathodic direction of the onset potential as shown in **Figure 3**. In these measurements, we performed two cycles at each anodic potential and the data shown were taken from the second cycle, where both the anodic and cathodic scan corresponds to the sample being subjected to the given anodic potential. As can be seen in Figure 3, the onset potential is quite constant until the anodic potential limit reaches 0.2 V_{RHE}. At more positive anodic potentials, there is a clear shift of the onset potential in the cathodic direction. With an anodic potential limit of 0.5 V_{RHE}, the onset potential was shifted more than 140 mV. By changing the anodic potential limit back to -0.3 V_{RHE}, the onset potential was restored to about -0.42 V_{RHE} (close to the initial value shown in Figure 3) within a few cycles.

The experimental results show that MXenes, and in particular vacancy-ordered $W_{1.33}C$, are promising material candidates for HER. The continuous improvement of the onset thanks to the use of high cathodic potential is very interesting. To explain this observation, we turn to first-principles calculations and analysis.
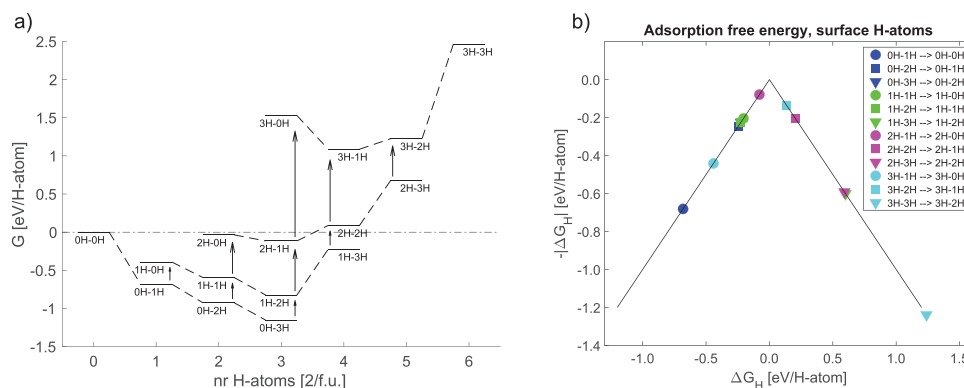
**ADVANCED
SCIENCE NEWS**
www.advancedsciencenews.com

**ADVANCED
SUSTAINABLE
SYSTEMS**
www.advsustainsys.com

Figure 4. a) Energy landscape, showing the relative energies of all configurations of adsorbed H on $W_{1.33}C$. The dashed lines mark adsorption on surface sites and arrows mark the migration of H (protons) from the surface to the vacancies. Calculated values for the adsorption energy can be found in Table S3 (Supporting Information), while the values for migration energies are found in Table S5 (Supporting Information). b) The adsorption free energy of surface bound H atoms on $W_{1.33}CO_2$ presented in the form of a volcano plot. Points on the left leg are stable, while those on the right are unstable (and should desorb).

2.3. Adsorption Free Energy

We calculate all possible configurations of H adsorbates on the surface and in the vacancies of the $W_{1.33}C$ MXene, fully terminated with O. For details on the adsorption configurations, see computational details and Supporting Information. The resulting energy landscape is presented in **Figure 4**a. Along the x-axis is the total number of H atoms in the system, while the energy is listed on the y-axis. The labels xH-yH mark the specific stoichiometry of adsorbates, with x H in each vacancy and y H on the surface (per side). The 0 level of the energy is defined based on the system without any H, or 0H-0H and is marked for reference in the figure by the dash-dotted line. The dashed lines follow adsorption of H onto the surface, the adsorption energy being defined by Equation (1) in the section on computational details. As the total amount of H increases with adsorption, this process also moves the system toward the right in the figure. The arrows mark the migration of H from the surface to the vacancies, as defined by Equation (5) in the computational details, and it represents the stability of H inside the vacancy, relative to adsorbed on the surface. As the migration keeps the total number of H constant, the shift of the system through migration is only vertical inside this figure. As can be seen, the adsorption of H onto the surface is favorable, until it is fully saturated, with the most stable state being 0H-3H. Beyond this, any migration of H atoms into the vacancy or adsorption of H directly into the vacancy is clearly unfavorable, more on migration energy in the next section.

In addition, for optimal HER we would need the adsorption free energy of hydrogen to be as close to zero as possible. Figure 4b shows the theoretical onset potential as a function of the adsorption free energy of surface H for different configurations of xH-yH, i.e., in the form of a volcano plot. The figure shows the adsorption free energy of surface H, while equivalent data for vacancy H is provided in the Supporting Information (the same data is part of the energy landscape of Figure 4a). In the volcano plot, any points on the left leg indicate a stable state, while the points to the right are unstable. There are points on both slopes of the diagram, for instance, we note that the adsorption energy of 0H-1H, which is furthest to the left, has a

value of −0.68 eV, which is not surprising given how unstable a purely O terminated structure is, and as such it would strongly favor adsorption of hydrogen. 2H-3H and 3H-3H are examples of unstable adsorptions far to the right of the diagram, with adsorption energies of 0.59 and 1.24 eV H-atom^{-1}, respectively. There are also a number of points close to the peak of the structure, with configurations 2H-1H (−0.08 eV H-atom^{-1}), 2H-2H (0.20 eV H-atom^{-1}), and 3H-2H (0.14 eV H-atom^{-1}).

We observe, however, a general trend in the adsorption energy, namely that structures that contain few H atoms tend to end up on the left side, and structures containing many H atoms tend to end up on the right side of the volcano plot. If we compare with the data on vacancy H provided in the Supporting Information, we also note that H atoms adsorbed to the O atoms on the surface tend to be further to the left than the ones in the vacancy.

2.4. Migration Energy

The relative stability of H atoms in the vacancy compared to adsorbed on the surface was evaluated based on the migration energy, as defined in the methods section below (Equation (5)), and presented in Figure 4a, through the vertical arrows. In all cases the migration energy for H moving from the vacancy to the surface is negative, meaning that H in the vacancy is not thermodynamically stable compared to being bonded to the O atoms on the surface. It also demonstrates that the more H there are in the vacancies, relative to on the surface, the more unstable the configuration becomes. For example, the least stable configuration for the migration of a single H atom is 3H-0H, using the short form notation for 3H in the vacancy, and 0H on the surface, such that the vacancies are fully occupied by H, and with none bonded to O on the surface. The energy difference of one of those H atoms migrating from the vacancy to the surface and into configuration 2H-1H is as high as −1.64 eV H-atom^{-1}. Even in the more favorable configurations, such as 1H-0H, or 1H-2H, the migration energy is still negative at ≈−0.3 eV H-atom^{-1}. This shows that any occupancy of H in the vacancy sites is energetically unfavorable compared

**ADVANCED
SCIENCE NEWS**

www.advancedsciencenews.com

**ADVANCED
SUSTAINABLE
SYSTEMS**

www.advsustainsys.com

to vacant surface sites. However, a cathodic potential, which changes the energy reference with respect to protons, can provide enough driving force for protons to occupy the vacancies. Given computational hydrogen electrode (CHE) and thermodynamical considerations, this will occur once the cathodic potential is equal to the Gibbs free absorption energy of H in the vacancy sites. The migration of protons to the vacancy sites will be assumed to be associated with low barriers.[29,30] Once at the vacancy site the proton will gain an electron, thereby transforming to an absorbed hydrogen atom. As long as sufficiently cathodic potentials are maintained, the H atoms remain stable in those states. The presence of energy barriers (more on that below) can prevent H atoms from migrating from the vacancy sites to the surface sites, and, further, if the surface sites are filled there is no position to migrate to. There may still be the possibility for desorbing entirely, through the adsorption free energy of H in vacancy states, see the Supporting Information.

2.5. Energy Barriers

Even though the presence of H in the vacancies is energetically unfavorable, the existence of energy barriers may allow metastable states of such configurations. To investigate such potential barriers, we have carried out nudged elastic band (NEB) calculations to try to find a minimum energy path (MEP) for H atoms moving from the vacancies to the surface. We then consider the migration of 2 H atoms, one per side of the vacancy-ordered MXene. The energy is presented per f.u., so the difference between endpoints refers to the migration energy per 2 H atoms. Examples of these MEPs, and barriers, are provided based both on configurations of low as well as high total migration energy, see **Figure 5**. Black stars mark calculated data points obtained in the NEB, while the curves are interpolations from the calculated values. The configuration 1H-2H and 1H-0H both have low migration energies and are amongst

the most stable vacancy configurations, while 3H-0H has the highest migration energy and is most unstable with respect to migration of a single H atom to the surface.

Figure 5 shows the MEPs for these select configurations. From configuration 1H-2H → 0H-3H (blue in the figure), the single H in the vacancy migrates up to the surface, after which the surface sites are fully occupied by H atoms and the vacancies are empty. According to Figure 4a, and data in Table S5 in the Supporting Information, it has a migration energy of −0.33 eV H-atom^{-1}. The figure indicates two distinct peaks on the path, with a valley between them. Each peak represents the migration of a single H atom, as the process involves one H per side migrating and in our calculations they do so one at a time. The valley between peaks then represents the state where one H has completed the transition to the surface, while the second is still in the vacancy. Thus, the peaks, with a size of ≈1 eV blocks the migration of a single atom, while the energy difference between the two end states of 0.66 eV applies to the full transition of two H atoms. The MEP for 1H-0H → 0H-1H (green in the figure), display a similar structure of twin peaks. This one has an energy difference between end states of 0.29 eV H-atom^{-1}, with a large barrier of ≈1.5 eV blocking the migration of each hydrogen atom. Additional calculations on other migration paths, show barriers of about the same size as the MEP for 1H-2H. As a final example, we include the MEP of 3H-0H → 2H-1H (red in the figure). This one has the highest migration energy of all those considered, about −1.64 eV H-atom^{-1}, and is expected to be highly unstable. Even here the MEP contains a barrier of ≈1.5 eV for the migration of the first hydrogen atom. There is a weak signature of a second peak around point 5 for the transition of the second hydrogen atom, indicating that the migration of both hydrogen atoms is mainly determined by the first migration, or rather that the total slope is so pronounced that the second peak disappears in it.

We now see that although H atoms in the vacancy are clearly thermodynamically unfavorable, compared to their surface states, the barriers are more than sufficient to prevent the immediate migration, rendering them metastable. This metastability should persist as long as they are bonded as H atoms, but given an anodic potential, they will revert to H$^+$ ions (protons) which would be unaffected by the barriers and free to migrate out.

3. Conclusions

Experiments on HER for Mo-, W-, and Nb-based MXenes show promising results for HER activity, in particular for the W$_{1.33}$C MXene with ordered vacancies, where we also observed significant improvements in the onset potential during repeated cycling of cathodic potential. Therefore, this MXene was given additional attention through an extended experimental study of the onset potential and related first-principles calculations.

In order to observe changes in activity and onset potential, the potential was cycled from a potential more anodic than the HER onset to a potential in the HER region. It was shown that changing the potential limit from −0.5 to −0.75 V$_{RHE}$ leads to a significant increase in HER activity and a shift in the anodic direction of the onset potential by about 0.2 V was observed. Increasing the anodic potential limit to above 0.2 V$_{RHE}$ was
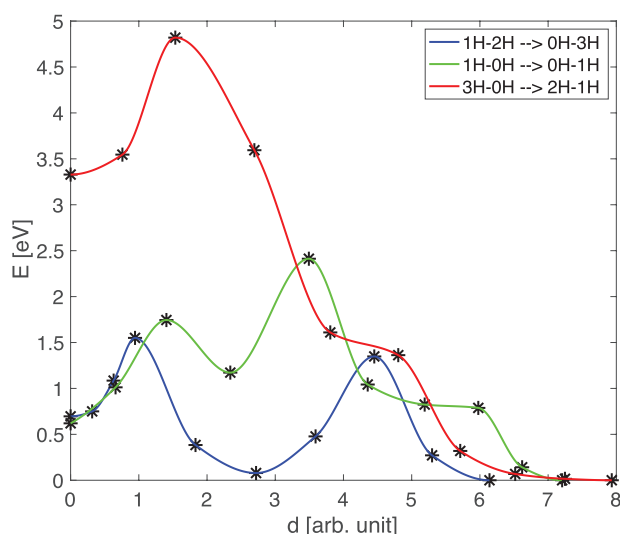

Figure 5. Minimum energy paths (MEP) for H atom migration. The black stars are calculated points from the MEP version, while the curves are PCHIP fitted interpolations. The energy is presented along the y-axis, while the migration distance in arbitrary units is presented along the x-axis.

shown to give the opposite effect, with a dramatic decrease in activity and a shift in the cathodic direction of the onset potential. Based on results from the first-principles investigation, we make the hypothesis that hydrogen can adsorb inside the vacancy, as well as on the surface. While we conclude that adsorption inside the vacancy is energetically unfavorable, compared to surface sites, we also suggest that under appropriate electrochemical conditions (large cathodic potential) these vacancy sites can become occupied via proton transfer. Once in the vacancy site the proton transforms into a chemically bound H atom. There are significant energy barriers preventing H atoms to diffuse back to the surface, allowing for the existence of this metastable state. A consequence of hydrogen in the vacancies is that the adsorption free energy of surface H atoms approaches thermoneutral values that leads to a shift in the anodic direction of the theoretical onset potential, which is observed in the experimental analysis. Also, as the occupancy of the vacancies increases the process is slowed down. Consequently, it takes more time, or repeated cycling, for enough H to adsorb inside the vacancy, and for the HER to reach its optimal potential, explaining the recorded improvements in the HER experiments. At anodic conditions, the electron will leave the hydrogen, forming a H^+ ion (proton), which will again be able to leave the vacancy. This will lead to a less thermoneutral adsorption free energy of H and consequently a shift in the cathodic direction of the onset potential, which is in line with experimental observation. In light of the agreement between experimental observations and first-principles results, this suggests that our hypothesis of hydrogen inside the vacancy is correct and that these additional adsorption sites contribute to increasing the hydrogen evolution reaction in the $W_{1.33}C$ vacancy MXene.

Owing to the high surface area and the possibility to further minimize the onset potential of the new family of vacancy-ordered MXenes, there is a real opportunity to use these materials as cathode materials in HER. Furthermore, the reversible structure changes suggested to occur in these MXenes can be explored further, for instance, as hydrogen storage material and/or as hydrogen separation membranes.

4. Experimental Section

Materials Synthesis—MAX Phase Synthesis: Five MAX phases and one MAX-phase-like material (Mo_2Ga_2C) were used as parent materials for MXene derivation. All phases except Mo_2Ga_2C were synthesized by mixing elemental powders in desired stoichiometric ratios and placing the mixture in a covered Al_2O_3 crucible. The latter was placed in an alumina tube furnace, through which Ar gas was flowing, it was heated at a specific rate to a certain temperature and was held at that temperature for a certain time. After cooling, the lightly sintered samples were crushed in an agate mortar, resulting in a fine powder of particle size below 30 μm. Synthesis conditions for each MAX phase are shown in **Table 1**.

Mo_2Ga_2C powders were synthesized by mixing -325 mesh Mo_2C powder with molten Ga (both obtained from Alfa Aesar, Ward Hill, MA, both of purity 99.5 wt%) in the ratio of 1:8. The mixture was placed in a quartz tube that was evacuated and sealed, further details can be found in ref. [33]. The latter was placed in a horizontal tube furnace that was heated at a rate of 10 °C min^{-1} to 850 °C, and was held at that temperature for 48 h. After cooling, the sample was crushed using an agate mortar and pestle then returned to the quartz tube, which was evacuated, sealed, and reheated in the horizontal furnace at a rate of 10 °C min^{-1} to 850 °C and held at that temperature for an additional 16 h. The produced sample was immersed in 12 M HCl (technical grade, Fisher Scientific, Fair Lawn, NJ) for 48 h, at room temperature (RT), while being stirred using a Teflon coated magnetic stirrer on a stir plate to dissolve any unreacted Ga.

Materials Synthesis—MXene Synthesis: All MXenes were synthesized by adding a certain amount of the MAX phase powder to a LiF (90 wt%, Alfa Aesar) + HCl solution in a Teflon bottle, and by stirring using a Teflon coated magnetic stirrer for a desired time at a certain temperature. When using a temperature above RT, an oil bath is used to maintain the desired temperature. Afterward, the mixture was washed through three cycles of 1 M HCl, followed by 3 cycles of 1 M aqueous LiCl (98 wt%, Alfa Aesar), and finally several cycles of DI water until the supernatant reached pH of ≈6. In each washing cycle, the washing was performed by adding 40 mL of the solution to the powder in a centrifuge tube, being hand-shaken for 1 min before centrifuging at 5000 rpm for 2 min, after which the supernatant is discarded. As the subsequent step, the MXene powders were delaminated by mixing the powder with 20 mL N_2 deaerated distilled water (DI), being hand-shaken for 5 min prior to sonication using an ultra sonic bath with N_2 bubbled through the suspension for 30 min, followed by centrifuging at 500 rpm for 10 min. The exact etching conditions for each MXene are described below in **Table 2**. All MXene colloidal suspensions were of a concentration between 1 and 0.5 mg mL^{-1}. Before electrochemical testing, the MXene colloidal suspension (5 mg) was mixed with Nafion 117 solution (≈5%; 5 μL) in ethanol (500 μL) using sonication for 5 min as described in more detail in ref. [15].

Electrochemical Experiments: The colloidal MXene suspensions, prepared as described above, were diluted with 18.2 MΩ cm Millipore water through sonication and was then drop-casted onto a glassy carbon (GC) disk (5 mm diameter, SIGRADUR G from HTW Hochtemperatur-Werkstoffe GmbH) substrate and dried under flowing Ar. The mass

Table 1. Synthesis conditions for the various MAX phases used.

MAX Phase	Elements and Stoichiometry	Synthesis conditions	Ref.
$(W_{2/3}Sc_{1/3})_2AlC$	4/3W (12 μm, Sigma-Aldrich): 2/3Sc (−200 mesh Standford Advanced Material): 1Al: 1C (both Al and C are −200 mesh from Alfa Aesar)	Heating rate: 8 °C min^{-1} Holding temperature: 1450 °C for 2 h	[9]
$(W_{2/3}Y_{1/3})_2AlC$	4/3W: 2/3Y (−400 mesh):1Al:1C	Heating rate: 8 °C min^{-1} Holding temperature: 1450 °C for 2 h	[9]
$(Mo_{2/3}Sc_{1/3})_2AlC$	4/3Mo (Sigma-Aldrich): 2/3Sc:1Al:1C	Heating rate: 5 °C min^{-1} Holding temperature: 1500 °C for 20 h	[8]
$(Mo_{2/3}Y_{1/3})_2AlC$	4/3Mo:2/3Y:1Al:1C	Heating rate: 10 °C min^{-1} Holding temperature: 1500 °C for 2 h	[31]
$(Nb_{2/3}Sc_{1/3})_2AlC$	4/3Nb (−325 mesh, alfa Aesar, Kandel, Germany, 99.8 wt%):2/3Sc:1Al:1C	Heating rate: 5 °C min^{-1} Holding temperature: 1400 °C for 2 h	[32]

**ADVANCED
SCIENCE NEWS**

www.advancedsciencenews.com

**ADVANCED
SUSTAINABLE
SYSTEMS**

www.advsustainsys.com

Table 2. Etching conditions for the used MXenes.

MAX phase etched	MXene produced	Etching conditions	Ref.
3 g $(W_{2/3}Sc_{1/3})_2AlC$	$W_{1.33}CT_z$ (Sc)	6 g LiF + 50 mL 12 M HCl for 48 h at RT	
3 g $(W_{2/3}Y_{1/3})_2AlC$	$W_{1.33}CT_z$ (Y)	6 g LiF + 50 mL 12 M HCl for 48 h at RT	
3 g $(Mo_{2/3}Sc_{1/3})_2AlC$	$Mo_{1.33}CT_z$ (Sc)	6 g LiF + 50 mL 12 M HCl for 48 h at RT	[8]
3 g $(Mo_{2/3}Y_{1/3})_2AlC$	$Mo_{1.33}CT_z$ (Y)	6 g LiF + 50 mL 12 M HCl for 48 h at RT	
3 g $(Nb_{2/3}Sc_{1/3})_2AlC$	$Nb_{1.33}CT_z$ (Sc)	6 g LiF + 50 mL 12 M HCl for 48 h at 35 °C	
2 g Mo_2Ga_2C	Mo_2CT_z	6 g LiF + 50 mL 12 M HCl for 336 h at 35 °C	[34]

loading for the active materials is 0.03 mg mL^{-1} and a volume of 0.1 mL was added to each electrode. The samples were mounted in a rotating disk electrode (RDE) rotor (Pine Research Instrumentation). HER activity was measured through polarization curves recorded in a standard three-electrode electrochemical cell with the rotating GC disc as working electrode, a graphite rod (3 mm, purity >99.995% from Sigma-Aldrich) as counter electrode and a Hg/Hg_2SO_4 reference electrode (B3610+ from SI Analytics). All potentials reported herein were converted to the reversible hydrogen electrode (RHE) scale. The RHE potential was measured experimentally after the HER evaluation of the MXene materials by cycling a Pt wire between −0.71 and −0.68 V versus the reference electrode in H_2-saturated 0.5 M H_2SO_4. The value of the RHE potential was assumed to be the intercept with the current axes as this value represents the reduction/oxidation potential for hydrogen (the RHE zero). The obtained RHE potential was found to be −0.696 V versus Hg/Hg_2SO_4. The electrochemical measurements were performed using a SP-300 potentiostat (Bio-Logic Science Instruments), controlled from a computer using the EC-Lab software.

All measurements were carried out in 0.5 M H_2SO_4 prepared from 96% H_2SO_4 (Suprapur grade, Merck) and 18.2 MΩ cm Millipore water. Prior to the experiments, the electrochemical glass cell and gas bubbler were cleaned in aqua regia overnight and rinsed thoroughly with 18.2 MΩ cm Millipore water to remove traces of noble metals, such as Pt which can be present on glass from previous experiments.

Electrochemical impedance spectroscopy (EIS) was used to estimate the Ohmic resistance. At high frequencies, the real part of the impedance is mainly due to the series resistance of the system, and the imaginary part relates to capacitive effects and charge transfer. Thus, it is possible to estimate the built-in series resistance by taking the intersection of the linear regression of the imaginary impedance to the axis of the real impedance in a Nyquist plot.[35] EIS was performed at open circuit potential in the frequency range of 10–50 000 Hz. Typical values for the measured Ohmic resistance, R_U, ranged from 5 to 8 Ω. The measured R_U values were used to iR-compensate the potential to 85% during the measurements and the remaining 15% were corrected for in the data analysis for the potentiodynamic experiments but left uncorrected for the potentiostatic experiments.

Computational Details: In a traditional MXene, such as Ti_2C and Mo_2C, the dangling bonds on the transition metal (TM) atoms are saturated by terminations, such as O, F, and OH. Whether there is a preference for O or F tends to depend on the valency of the TMs involved, as O requires 2 electrons and F only 1 electron to fill their respective shell.[36,37] OH groups have the same effective valency as F, and generally display similar bonding characteristic and electronic properties in simulations.[1,38] Given the example of the hypothetical structure of a regular W_2C MXene, fully terminated with O atoms into (W_2CO_2), each W is sixfold bonded with 3 C and 3 O, while each C is sixfold bonded with 6 W, and each O is threefold bonded with 3 W. There is (formally) a sufficient number of available electrons from the W atoms to occupy the empty orbitals of both the C and O atoms.[39] However, when metal vacancies are introduced to realize $W_{1.33}C$ MXene,[9] some of the W−C as well as W−O bonds are broken, so that each C binds with only 4 W and each O binds with only 2 W. In total, there are fewer electrons from W available to fill the empty C and O orbitals, leading to a preference for F or OH terminations over O in both $W_{1.33}CO_2$ and

$Mo_{1.33}CO_2$ along with indications of structural and dynamical instability in the fully O terminated variants.[39,40]

Given the above, for low concentration of F terminations a strong affinity for H adsorbates on top of O terminated vacancy-ordered MXenes were surmised, to instead form OH groups. See **Figure 6**a) for an illustration of this surface bonding. Furthermore, the presence of vacancies due to the removal of select W atoms has resulted in broken bonds for the C atoms. The possibility of capturing H atoms also inside
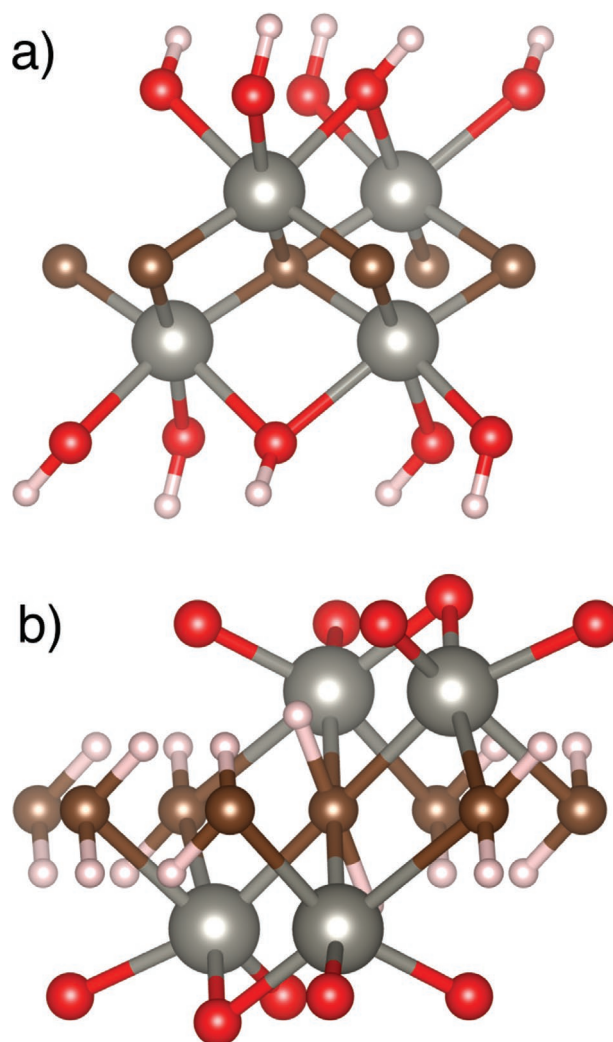

Figure 6. Illustration showing the atomic structure of $W_{1.33}CO_2$, a) for H atoms adsorbed to O on the surface, and b) to the C in the vacancy. In a) each O bonds with 1 H and in b) each C bonds with two H. Brown, gray, red, and white spheres correspond to C, W, O, and H, respectively.

**ADVANCED
SCIENCE NEWS**

www.advancedsciencenews.com

**ADVANCED
SUSTAINABLE
SYSTEMS**

www.advsustainsys.com

the vacancy, to be bonded to the C atoms and thereby substitute the broken C—W bonds is therefore proposed. Accordingly, a maximum of 3 H atoms per vacancy is considered, one for each broken C—W bond, see exemplified schematic in Figure 6b). This is in addition to the bonding sites on top of the O atoms, three per MXene side and primitive cell. In total, per primitive cell, there would be 6 potential bonding sites in the vacancies and 6 on the surfaces.

Calculations were carried out using DFT calculations, as implemented in the Vienna ab-initio Simulation Package (VASP) code.[41,42] The exchange-correlation effects were treated within the generalized gradient approximation (GGA) of Perdew–Burke–Ernzerhof.[43] Cutoff energy for the plane-wave expansion was 400 eV. The k-point sampling was adjusted for the supercell size to ensure an accuracy of at least 1 meV per H-atom during structural relaxations. Accordingly, a $15 \times 15 \times 1$ mesh was used during relaxation of 1×1 $W_4C_3O_6$ supercell size. A total supercell height of 36 Å was used to avoid self-interaction between MXene sheets across the periodic boundaries. With a total MXene sheet thickness of about 6 Å, including H atoms, the vacuum spacing is $\approx$30 Å.

Phonon calculations were carried out using density functional perturbation theory (DFPT), as implemented in VASP and PhonoPy codes.[44] Generated supercells have a size of $3 \times 3 \times 1$ primitive cells, the k-point mesh was chosen as a $3 \times 3 \times 1$ and the plane-wave expansion cutoff was set to 600 eV. From these supercell calculations, total and partial zero-point energy (ZPE) for select atoms could be determined.

The use of the computational hydrogen electrode (CHE), where the total energy of $1/2$ H_2 (in the gas phase, under standard conditions) equals that of $H^+ + e^-$,[45,46] allows for connecting the Gibbs free energy of adsorbed/absorbed hydrogen with the HER and the operating potential. In practice, this means that the stability of hydrogen, both at the surface and at the vacancy, becomes more stable with increasing cathode potentials, following a linear dependence. This simple electrochemical framework does not allow for calculations of electrochemical barriers, thus, the electrochemical analysis includes only thermodynamical considerations. In fact, barriers for proton transfer will be assumed to be small,[29,30] whereas the barriers for diffusion of hydrogen atoms will be calculated according to the computational details above.

MXene Supercell: Although it is expected that the vacancy-ordered MXene may have mixed terminations, including also F, previous theoretical work on hydrogen evolution in Ti-based MXene suggest primarily O or OH terminations[12,14] and that F drastically reduces the catalytic activity.[19] This is consistent with here performed test calculations for a F terminated surface. The results of which are summarized in the Supporting Information and Figure S1 (Supporting Information), and show that F functionalization drastically increases the adsorption energy of H atoms by more than 1 eV per H-atom compared to O. This makes any F functionalization a non-reactive site which can be expected to reduce overall HER activity, for the material investigated herein. Consequently, the theoretical analysis is limited to a MXene fully terminated by O atoms, $W_{1.33}CO_2$, on which H atoms can be adsorbed. Also, an O atom with an adsorbed H has the same valency as F, and thus it can be expected to behave similar to a F termination in its interaction with other OH groups. In addition, for $W_{1.33}CO_2$ it is assumed that all O atoms are situated in the "edge", or "near A" sites, suspended between two W atoms in the closest M-plane and above the W atoms in the opposite plane, as described in more detail in the previous work,[39,40] see also Figure S2 in the Supporting Information. A varying number of H atoms are distributed and bound to the O atoms on the surface and to the C in the vacancies, under the constraint that the number of H atoms on either side of the MXene sheet remain equal. A primitive cell of $W_{1.33}CO_2$ contains 4 W atoms, 3 C atoms and 6 O atoms (3 on either side), and is three times larger, with the sides $\sqrt{3}$ times longer, than the primitive cell of W_2CO_2, which is a consequence of the ordered vacancies and a reduced symmetry. An approximate C—H bond length of $\approx$1.1 Å is predicted, while the typical H-H atomic distance inside the vacancy is around 1.7–2.0 Å. As such, there is sufficient spacing between the H atoms for H—H bonds not to form. The bond length in an H_2 molecule is known to be 0.74 Å.

The possibility of having different number of H atoms is considered in both the vacancy and on the surface, and the terminology $3 \cdot W_{1.33}C: 2 \cdot (xH\text{-}O_3\text{-}\gamma H)$ is used, or in short form just xH-γH, to label a specific stoichiometry/configuration of H atoms. Here, "x" refers to the number of H atoms per vacancy (0-3 per side, twice that number for the primitive unit cell) and "y" refers to the number of H atoms adsorbed to the O atoms on the surface to form OH (0-3 per side, double that for the primitive unit cell). The same number of H atoms per side is always considered, in vacancies and on the surface, and the numbers x and y refers to the number per side (half of the total per primitive cell). For a specific number of H atoms, these atoms can be arranged in multiple configurations. With 0 or 3 atoms per vacancy/surface there is only 1 possible configuration, while 1 or 2 atoms can be arranged in 3 different ways per side, 9 in total considering both sides. With H in both vacancies and on the surface, 1 or 2 H per vacancy/surface results in a total of 81 configurations, even though several of them are symmetrically equivalent. All possible configurations are considered and the equilibrium states of each are determined individually to identify the one with the lowest possible energy, which thereafter is used to represent that particular stoichiometry. More details, along with diagrams (Figure S2, Supporting Information) and tables (Table S1, Supporting Information) defining those representative configurations are provided in the Supporting Information.

Free Energy of Hydrogen Adsorption: The adsorption free energy of H atoms is defined as the difference in energy between H adsorbed on the MXene and as free H_2 molecules. It is evaluated both for the atoms bonded in the vacancy and the ones bonded on top of the O atoms on the surface. The adsorption free energy ΔG_H for a single adsorbed H atom, with free H_2 molecules as a reference point, is described according to the following formula

$$\Delta E_H = \frac{E(3 \cdot W_{1.33}C : 2 \cdot (x'H - O_3 - \gamma'H)) - E(3 \cdot W_{1.33}C : 2 \cdot (x''H - O_3 - \gamma''H)) - E(H_2)}{2} \quad (1)$$

$$\begin{aligned} x' = 0,1,2,3 \quad & \gamma' = 0,1,2,3 \quad x' + \gamma' = 1,2,\ldots 6 \\ x'' = 0,1,2,3 \quad & \gamma'' = 0,1,2,3 \quad x'' + \gamma'' = x' + \gamma' - 1 \end{aligned} \quad (2)$$

$$\Delta G_H = \Delta E_H - T\Delta S_H + \Delta ZPE \quad (3)$$

$$T\Delta S_H = -0.2 \text{ eV Hatom}^{-1} \quad (4)$$

$$\Delta ZPE = \begin{cases} 0.27 - 0.27/2 = 0.135 \text{ eV Hatom}^{-1} & \text{(in a vacancy)} \\ 0.29 - 0.27/2 = 0.155 \text{ eV Hatom}^{-1} & \text{(on the surface)} \end{cases} \quad (5)$$

In this equation, $E(3 \cdot W_{1.33}C: 2 \cdot (x'H - O_3 - \gamma'H))$ is the energy of the $W_{1.33}CO_2$ with a configuration of x' H in the vacancy and y' H on the surface. $E(3 \cdot W_{1.33}C: 2 \cdot (x''H - O_3 - \gamma''H))$ is the energy of the same $W_{1.33}CO_2$, but with 2 adsorbed H atoms, one per side, removed from the vacancy or the surface. $E(H_2)$ is the energy of a gas-phase H_2 molecule. The complete formula is divided by 2 to get the energy per H atom. It is assumed that the vibrational entropy for adsorbed H atoms is negligible, so that the change in entropy is based solely on the vibrational free energy of molecular hydrogen, and $T\Delta S_H$ is constant at -0.2 eV H-atom^{-1}.[15] In addition, ΔZPE is the difference in ZPE between bound H atoms and free H_2 molecules. The ZPE of adsorbed H is mentioned in the previous section and the ZPE of a free H_2 molecule is known to be 0.27 eV per molecule.[45]

Volcano Plots: The adsorption free energy of H is an important descriptor for HER. For instance, it is a necessary, but not sufficient, condition for fast evolution that the adsorption free energy is close to zero.[15,45] This is a natural consequence of the use of CHE. If the adsorption energy is positive, the reaction is endothermic and the H atoms will not bind, and if it is negative, the process is exothermic, and then the atoms will be unable to leave the surface. This is usually presented in the form of a volcano diagram, which plots the Gibbs free energy of H atoms along the x-axis, against calculated overpotential, which for HER and under premises set by the CHE is negative

magnitude of the Gibbs free energy, along the y-axis.[45,46] Ideally, the data point for a particular structure should be as close to the peak as possible if it should be considered as a promising candidate for HER. For a corresponding experimental approach, the theoretically predicted free energy along the x-axis is plotted against the experimental catalytic current on the y-axis. In the theoretical version, as demonstrated here, the data points for multiple materials lie, per definition, on a perfect triangle, while any experimental results should approximate this triangle. In addition, it is noted that points lying on the left leg of the diagram represent stable states, where the adsorption is exothermic and H atoms would not spontaneously be released from the surface, while any points on the right leg have positive adsorption energy leading to unstable states where the bonded H would spontaneously leave the surface, either in the form of hydrogen gas or as a proton depending on the applied potential.

Migration Energy: The migration energy of H atoms is defined as the change in free energy as H atoms move, or migrate, from adsorption sites in the vacancies to ones on the surface. To calculate this, the following equation is used

$$E_{migr} = \frac{E\left(3 \cdot W_{1.33}C : 2 \cdot \left((x-1)H - O_3 - (y+1)H\right)\right) - E\left(3 \cdot W_{1.33}C : 2 \cdot (xH - O_3 - yH)\right)}{2} \quad (6)$$

$$G_{migr} = E_{migr} + \Delta ZPE \quad (7)$$

$$\Delta ZPE = 0.29 - 0.27 = 0.02 \text{ eV Hatom}^{-1} \quad (8)$$

Here $E(3 \cdot W_{1.33}C : 2 \cdot (xH - O_3 - yH))$ is the energy of some configuration xH-yH, where $x = 1, 2, 3$ and $y = 0, 1, 2$. These ranges are given since there has to be at least one atom in the vacancies, and one empty space on the surface, for the migration to occur. $E(3 \cdot W_{1.33}C: 2 \cdot ((x-1)H - O_3 - (y+1)H))$ is the energy after migration of one H per side from the vacancy to the surface, such that the number of H in the vacancy is reduced by one and the ones on the surface have increased by one. Since the calculations were done with one migrating atom per side of the MXene, the difference is divided by two to get the migration energy per H atom. By this definition, if the migration energy is negative it means the H atoms would prefer to migrate to the surface. To get the migration free energy G_{migr}, it is also necessary to account for changes in vibrational free energy and the ZPE. Assuming the vibrational entropy is the same for surface and vacancy H, the change in vibrational free energy is 0. The ZPE for H atoms vary slightly depending on configuration and specific sites, but typical values are 0.29 eV atom^{-1} for H atoms adsorbed to the surface, and 0.27 eV atom^{-1} for those H inside the vacancy. Consequently, ΔZPE, the difference in ZPE, is $\approx$0.02 eV atom^{-1} from the migration from vacancy to surface.

Nudged Elastic Bands (NEB) Method: The minimum energy paths (MEP) for atom migrations between vacancy and surface states are calculated using the nudged elastic band method with climbing images as implemented in the VASP Transition State Theory (VTST) code.[47,48] A total of eight images were generated between the relaxed structures of the two metastable end states, and the MEP was relaxed using a 15 × 15 × 1 k-mesh. The initial path was generated as a linear interpolation, to the extent possible, but in cases where this would lead to atoms getting too close to one another, this was prevented by manually adding a "bend" to the path. In addition, since the two end states typically have different lattice parameters, a linear interpolation was applied. Unlike the internal atomic coordinates, the lattice parameters were not relaxed to optimal values along the path, but were kept fixed for each individual image. While methods for relaxing the lattice parameters along the path exists,[49] they are designed for bulk structures, and are not straightforward to implement in 2D structures like MXenes. The calculated data points were interpolated using Piecewise Cubic Hermite Interpolating Polynomial (PCHIP). The method was chosen since it resulted in a smooth curve and respected the extrema from the calculated data point.

Supporting Information

Supporting Information is available from the Wiley Online Library or from the author.

Conflict of Interest

The authors declare no conflict of interest.

[1] M. Naguib, M. Kurtoglu, V. Presser, J. Lu, J. Niu, M. Heon, L. Hultman, Y. Gogotsi, M. W. Barsoum, *Adv. Mater.* **2011**, *23*, 4248.

[2] M. Naguib, O. Mashtalir, J. Carle, V. Presser, J. Lu, L. Hultman, Y. Gogotsi, M. W. Barsoum, *ACS Nano* **2012**, *6*, 1322.

[3] M. W. Barsoum, *Prog. Solid State Chem.* **2000**, *28*, 201.

[4] Q. Hu, D. Sun, Q. Wu, H. Wang, L. Wang, B. Liu, A. Zhou, J. He, *J. Phys. Chem. A* **2013**, *117*, 14253.

[5] B. Anasori, M. R. Lukatskaya, Y. Gogotsi, *Nat. Rev. Mater.* **2017**, *2*, 16098.

[6] J. Halim, M. R. Lukatskaya, K. M. Cook, J. Lu, C. R. Smith, L.-Å. Näslund, S. J. May, L. Hultman, Y. Gogotsi, P. Eklund, M. W. Barsoum, *Chem. Mater.* **2014**, *26*, 2374.

[7] F. Shahzad, M. Alhabeb, C. B. Hatter, B. Anasori, S. Man Hong, C. M. Koo, Y. Gogotsi, *Science* **2016**, *353*, 1137.

[8] Q. Tao, M. Dahlqvist, J. Lu, S. Kota, R. Meshkian, J. Halim, J. Palisaitis, L. Hultman, M. W. Barsoum, P. O. Å. Persson, J. Rosen, *Nat. Commun.* **2017**, *8*, 14949.

[9] R. Meshkian, M. Dahlqvist, J. Lu, B. Wickman, J. Halim, J. Thörnberg, Q. Tao, S. Li, S. Intikhab, J. Snyder, M. W. Barsoum, M. Yildizhan, J. Palisaitis, L. Hultman, P. O. Å. Persson, J. Rosen, *Adv. Mater.* **2018**, *30*, 1706409.

[10] I. Persson, A. el Ghazaly, Q. Tao, J. Halim, S. Kota, V. Darakchieva, J. Palisaitis, M. W. Barsoum, J. Rosen, P. O. Å. Persson, *Small* **2018**, *14*, 1703676.

[11] P. Srimuk, J. Halim, J. Lee, Q. Tao, J. Rosen, V. Presser, *ACS Sustainable Chem. Eng.* **2018**, *6*, 3739.

[12] H. Pan, *Sci. Rep.* **2016**, *6*, 32531.

[13] M. Pandey, K. S. Thygesen, *J. Phys. Chem. C* **2017**, *121*, 13593.

[14] G. Gao, A. P. O'Mullane, A. Du, *ACS Catal.* **2017**, *7*, 494.

[15] Z. W. Seh, K. D. Fredrickson, B. Anasori, J. Kibsgaard, A. L. Strickler, M. R. Lukatskaya, Y. Gogotsi, T. F. Jaramillo, A. Vojvodic, *ACS Energy Lett.* **2016**, *1*, 589.

**ADVANCED
SCIENCE NEWS**

www.advancedsciencenews.com

**ADVANCED
SUSTAINABLE
SYSTEMS**

www.advsustainsys.com

[16] J. Zhu, E. Ha, G. Zhao, Y. Zhou, D. Huang, G. Yue, L. Hu, N. Sun, Y. Wang, L. Y. S. Lee, C. Xu, K.-Y. Wong, D. Astruc, P. Zhao, *Coord. Chem. Rev.* **2017**, *352*, 306.

[17] J. Zhang, Y. Zhao, X. Guo, C. Chen, C.-L. Dong, R.-S. Liu, C.-P. Han, Y. Li, Y. Gogotsi, G. Wang, *Nat. Catal.* **2018**, *1*, 985.

[18] D. A. Kuznetsov, Z. Chen, P. V. Kumar, A. Tsoukalou, A. Kierzkowska, P. M. Abdala, O. V. Safonova, A. Fedorov, C. R. Müller, *J. Am. Chem. Soc.* **2019**, *141*, 17809.

[19] A. D. Handoko, K. D. Fredrickson, B. Anasori, K. W. Convey, L. R. Johnson, Y. Gogotsi, A. Vojvodic, Z. W. She, *ACS Appl. Energy Mater.* **2018**, *1*, 173.

[20] T. Li, L. Yao, Q. Liu, J. Gu, R. Luo, J. Li, X. Yan, W. Wang, P. Liu, B. Chen, W. Zhang, W. Abbas, R. Naz, D. Zhang, *Angew. Chem., Int. Ed.* **2018**, *57*, 6115.

[21] T. Li, X. Yan, L. Huang, J. Li, L. Yao, Q. Zhu, W. Wang, W. Abbas, R. Naz, J. Gu, Q. Liu, W. Zhang, D. Zhang, *J. Mater. Chem. A* **2019**, *7*, 14462.

[22] M. H. Tran, T. Schäfer, A. Shahraei, M. Dürrschnabel, L. Molina-Luna, U. I. Kramm, C. S. Birkel, *ACS Appl. Energy Mater.* **2018**, *1*, 3908.

[23] Z. W. Seh, J. Kibsgaard, C. F. Dickens, I. Chorkendorff, J. K. Nørskov, T. F. Jaramillo, *Science* **2017**, *355*, eaad4998.

[24] T. F. Jaramillo, K. P. Jorgensen, J. Bonde, J. H. Nielsen, S. Horch, I. Chorkendorff, *Science* **2017**, *317*, 100.

[25] M. A. Lukowski, A. S. Daniel, F. Meng, A. Forticaux, L. Li, J. Song, *J. Am. Chem. Soc.* **2013**, *135*, 10274.

[26] G. Gao, J. Yan, M. Fengxian, J. Yalong, W. Eric, D. Aijun, *J. Phys. Chem. C* **2015**, *119*, 13124.

[27] C. Ling, L. Shi, Y. Ouyang, Q. Chen, J. Wang, *Adv. Sci.* **2016**, *3*, 1600180.

[28] P. C. K. Vesborg, B. Seger, I. Chorkendorff, *J. Phys. Chem. Lett.* **2015**, *6*, 951.

[29] S. Hu, M. Lozada-Hidalgo, F. C. Wang, A. Mishchenko, F. Schedin, R. R. Nair, E. W. Hill, D. W. Boukhvalov, M. I. Katsnelson, R. A. W. Dryfe, I. V. Grigorieva, H. A. Wu, A. K. Geim, *Nature* **2014**, *516*, 227.

[30] M. Seel, R. Pandey, *2D Mater.* **2016**, *3*, 025004.

[31] M. Dahlqvist, J. Lu, R. Meshkian, Q. Tao, L. Hultman, J. Rosen, *Sci. Adv.* **2017**, *3*, 1700642.

[32] J. Halim, J. Palisaitis, J. Lu, J. Thörnberg, E. Moon, M. Precner, P. Eklund, P. O. Å. Persson, M. W. Barsoum, J. Rosen, *ACS Appl. Nano Mater.* **2018**, *1*, 2455.

[33] C. Hu, C.-C. Lai, Q. Tao, J. Lu, J. Halim, L. Sun, J. Zhang, J. Yang, B. Anasori, J. Wang, *Chem. Commun.* **2015**, *51*, 6560.

[34] J. Halim, S. Kota, M. R. Lukatskaya, M. Naguib, M. Q. Zhao, E. J. Moon, J. Pitock, J. Nanda, S. J. May, Y. Gogotsi, *Adv. Funct. Mater.* **2016**, *26*, 3118.

[35] C. Wei, R. R. R. Rao, J. Peng, B. Huang, I. E. L. Stephens, M. Risch, Z. J. Xu, Y. Shao-Horn, *Adv. Mater.* **2019**, *31*, 1806296.

[36] M. Khazaei, A. Ranjbar, M. Arai, T. Sasaki, S. Yunoki, *J. Mater. Chem. C* **2017**, *5*, 2488.

[37] M. Khazaei, A. Mishra, N. S. Venkataramanan, A. K. Singh, S. Yunoki, *Curr. Opin. Solid State Mater. Sci.* **2019**, *23*, 164.

[38] M. Khazaei, M. Arai, T. Sasaki, C.-Y. Chung, N. Venkataramanan, M. Estili, Y. Sakka, Y. Kawazoe, *Adv. Funct. Mater.* **2013**, *23*, 2185.

[39] R. Meshkian, H. Lind, J. Halim, A. el Ghazaly, J. Thörnberg, Q. Tao, M. Dahlqvist, J. Palisaitis, P. O. Å. Persson, J. Rosen, *ACS Appl. Nano Mater.* **2019**, *2*, 6209.

[40] H. Lind, J. Halim, S. I. Simak, J. Rosen, *Phys. Rev. Mater.* **2017**, *1*, 044002.

[41] G. Kresse, J. Hafner, *Phys. Rev. B* **1994**, *49*, 14251.

[42] G. Kresse, J. Furthmüller, *Phys. Rev. B* **1996**, *54*, 11169.

[43] J. P. Perdew, K. Burke, M. Ernzerhof, *Phys. Rev. Lett.* **1996**, *77*, 3865.

[44] A. Togo, I. Tanaka, *Scr. Mater.* **2015**, *108*, 1.

[45] J. K. Nørskov, T. Bligaard, A. Logadottir, J. R. Kitchin, J. G. Chen, S. Pandelov, U. Stimming, *J. Electrochem. Soc.* **2005**, *152*, J23.

[46] J. Greeley, T. F. Jaramillo, J. Bonde, I. Chorkendorff, J. K. Nørskov, *Nat. Mater.* **2006**, *5*, 909.

[47] G. Henkelman, H. Jónsson, *J. Chem. Phys.* **2000**, *113*, 9978.

[48] G. Henkelman, B. P. Uberuaga, H. Jónsson, *J. Chem. Phys.* **2000**, *113*, 9901.

[49] D. Sheppard, P. Xiao, W. Chemelewski, D. D. Johnson, G. Henkelman, *J. Chem. Phys.* **2012**, *136*, 074103.